Materials Horizons

ROYAL SOCIETY OF CHEMISTRY

COMMUNICATION

View Article Online
View Journal | View Issue

Cite this: *Mater. Horiz.*, 2022, 9, 2443

Received 29th April 2022,
Accepted 20th June 2022

DOI: 10.1039/d2mh00537a

rsc.li/materials-horizons

Molecular logic operations from complex coacervation with aggregation-induced emission characteristics†

Jianhui Liu, [a] Tianfu Zhang, [b] Xiaolin Liu, [b] Jacky W. Y. Lam, [b] Ben Zhong Tang [bc] and Ying Chau *[a]

Leveraging complex coacervation of a polycation and a bivalent anion with aggregation-induced emission characteristics, we accomplish eight basic logic operations with environmental stimuli as inputs, producing Boolean-like fluorescence intensity or turbidity 'outputs' with contrast higher than one order of magnitude. Storage of information of a fluorescent pattern and thermo-sensor applications are also demonstrated.

New concepts

Molecular logic operations have been largely constructed as they exemplify the miniaturization of Boolean operations. However, most of the reported systems only performed limited types of basic logic operations or/and exhibited limited contrast between Boolean output signals. Here, simply exploiting the complex coacervation between a polycation and a bivalent anion with aggregation-induced emission characteristics, we accomplish all the eight basic logic operations, namely, 'Buffer', 'NOT', 'AND', 'OR', 'NAND', 'NOR', 'XOR' and 'XNOR', producing Boolean-like fluorescence intensity or turbidity 'outputs' with contrast higher than one order of magnitude. Moreover, a matrix of Buffer-type molecular logic gates is fabricated to store the information of a fluorescent pattern, and a solidified NOT-type logic gate in a hydrogel is exploited as a thermo-sensor of the surrounding solution. This work can help to boost the design of simple yet high-contrast molecular logic gates, together with the development of information storage media and environmental sensor devices.

Molecular logic operations are performed *via* molecular logic gates based on the 'digital' molecular response to changes in the environment,[1–3] wherein one or more binary inputs produce a single binary output.[4] Molecular logic gates have been constructed and investigated owing to their fundamental roles in the integration, processing and storage of information, as well as a wide array of applications spanning biosensors, environmental monitoring, and diagnosis of diseases.[1] A wide array of materials have been used as the building blocks of molecular logic gates, including small molecules,[5–7] polymers,[8] coordination materials[9] and biological materials,[10,11] which can be triggered by inputs with distinctive nature, including physical, chemical and biological stimuli.[12] In particular, the eight basic logic operations with single input ('Buffer'[13–19] and 'NOT'[16–18]) or two inputs ('AND',[5,13–16,19–24] 'OR',[13–15,17,22,23,25] 'NAND',[5,22–24,26,27] 'NOR',[17,22,23] 'XOR'[15,20,28,29] and 'XNOR'[28,30–33]) have aroused broad interest. To the best of our knowledge, these reports perform limited basic logic operations,[23,24,27,34] require complicated fabrication processes,[15,23] or exhibit limited contrast between outputs.[15,23,24,27,35] It will be promising if a concise and easy-to-make molecular system can achieve all basic molecular operations with high contrast between Boolean outputs.

Fluorescence has been widely used as an optical output of molecular logic operations owing to the ease of observation.[12,36] The well-known quenching effect of luminophores causes a decrease of fluorescence intensity (FI), affording the intrinsic nature of a NOT logic operation. Distinctively, aggregation-induced emission (AIE) is an unconventional photophysical phenomenon coined in 2001.[37–41] The AIE luminogens are non-emissive under the dispersed state; however, they become emissive under conditions of aggregation or restriction of intramolecular motion, and have been developed into smart materials[40] responsive to multifaceted stimuli such as mechanics, temperature, pH and light.[39] Coacervation, also known as liquid–liquid phase separation,[42] is a pivotal[43–45] way of intracellular organization of

[a] *Department of Chemical and Biological Engineering, the Hong Kong University of Science and Technology, Clear Water Bay, Kowloon, Hong Kong SAR, China. E-mail: keychau@ust.hk*

[b] *Department of Chemistry and Hong Kong Branch of Chinese National Engineering Research Center for Tissue Restoration and Reconstruction, the Hong Kong University of Science and Technology, Clear Water Bay, Kowloon, Hong Kong SAR, China*

[c] *School of Science and Engineering, Shenzhen Key Laboratory of Functional Aggregate Materials, the Chinese University of Hong Kong, Shenzhen, Guangdong 518172, China*

† Electronic supplementary information (ESI) available: Materials, methods, supplementary turbidity data, fluorescence intensity data and confocal laser scanning microscopy. See DOI: https://doi.org/10.1039/d2mh00537a

biomolecules and is fundamental to the formation of membraneless organelles.[46–50] The peculiar liquidity of membraneless organelles affords cells to host compartments with high dynamics, mobility, environmental responsiveness and reversibility.[51] Complex coacervation is the process of associative phase separation of oppositely-charged molecular species, generating a condensed phase (coacervate) and a dilute phase (dispersed phase).[52] We reason that complex coacervation with AIE luminogens (AIEgens) that otherwise do not self-aggregate can trigger prominent and environment-responsive enrichment of the dye. This would lead to restriction of the intramolecular motion of AIEgens and allow the excitons to decay radiatively. In this paper, leveraging a binary complex coacervation phenomenon comprising AIEgens, we demonstrate the construction of eight basic molecular logic operations with FI or turbidity as the digital-like Boolean outputs.

Polyelectrolytes can undergo complex coacervation with charge-complementary species,[52–54] particularly with counterionic bivalent small molecules as transient and weak 'cross-linkers' to mediate complex coacervation.[55] The arginine–glycine–glycine motif is widely presented in human proteins for molecular interactions including electrostatic attraction.[56] As such, we grafted dextran[57] with cysteine-terminated (arginine–glycine–glycine)-containing peptide (Ac–CGGRGG–$CONH_2$), to synthesize a dextran-CGGRGG hybrid (DCH) as the polycation (Fig. 1). For the counterionic partners, we synthesized 1,2-bis[4-(4-sulfonatobutoxyl)phenyl]-1,2-diphenylethene salt (BSBOTPE, Fig. 1), a bivalent, anionic and hydrophilic small molecule comprising tetraphenylethene with AIE characteristics.[58] Whilst the DCH or BSBOTPE alone remained dispersed in solution, the coexistence of DCH and BSBOTPE engendered coacervation in a stoichiometry-dependent and temperature-responsive manner with an upper critical solution temperature (UCST), as indicated by turbidimetry (Fig. S1A and C, ESI†). This UCST-type[59] phase behavior is consistent with a previous report of complex coacervation comprising hydrophilic polyelectrolytes.[60,61] Moreover, the presence of coacervation is concomitant with the surge of fluorescence in a coherent fashion (Fig. S1B and D, ESI†), as indicated by overall FI. These data suggest that the complex coacervation phenomenon could be exploited for molecular logic operations with environmental stimuli and chemicals as 'inputs', and FI or turbidity as 'outputs' with high contrast between '0' and '1' values.

Firstly, DCH and BSBOTPE were used as inputs to demonstrate Buffer and AND logic operations. The relative FI at 471 nm is viewed as the output with 0.5 as the threshold value. For a Buffer logic operation, the output ('0' or '1') is the same as the input ('0' or '1') (Fig. 2A and B). DCH alone was non-fluorescent (output = 0), whilst the addition of BSBOTPE generated complex coacervation and aggregation of BSBOTPE in coacervate phase, thereby producing high FI signal (output = 1) (Fig. 2C and D). The role of DCH and BSBOTPE can be switched to perform another Buffer logic operation (Fig. S2, ESI†). For an AND logic gate, the output is '1' only if both inputs are '1' (Fig. 3A and B). This scenario is well represented by the combination of BSBOTPE and DCH as the inputs, namely, only the coexistence thereof can generate '1' output owing to complex-coacervation-caused AIE (Fig. 3C and D). For an OR logic gate, the output is '1' if either of the inputs is '1' (Fig. 4A and B). We added an intrinsically disordered protein (IDP)-mimicking polymer-oligopeptide hybrid* (IPH*), which is

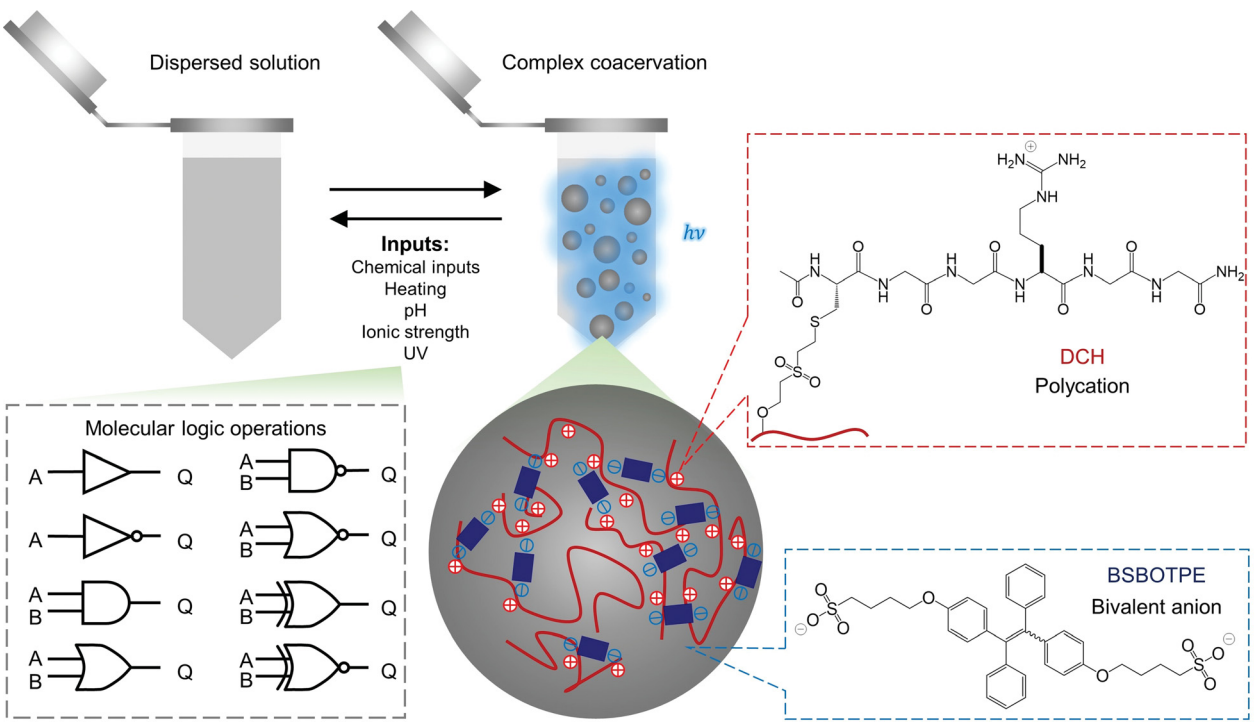

Fig. 1 Schematic illustration of complex coacervation and application for molecular logic operations thereof.

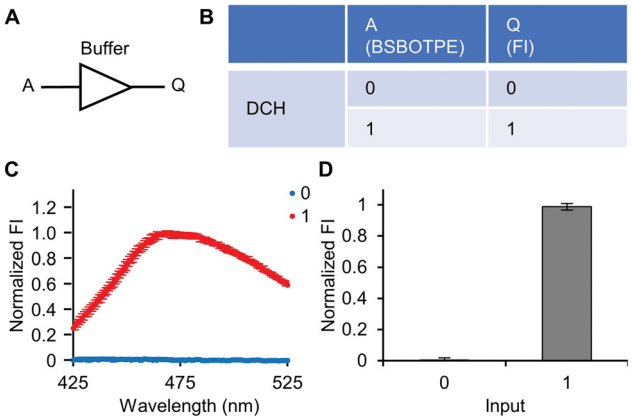

	A (BSBOTPE)	Q (FI)
DCH	0	0
	1	1

Fig. 2 Buffer logic operation. (A) Symbol of logic gate. (B) Truth table. (C) The normalized fluorescence spectra of logic operation with different inputs. (D) Normalized FI at 471 nm. The concentrations of DCH and BSBOTPE used are 6 μM and 141 μM, respectively. Excitation wavelength was set at 350 nm. n = 3.

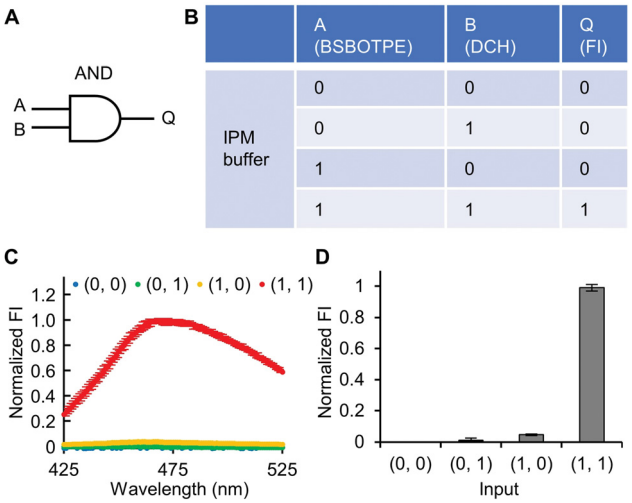

	A (BSBOTPE)	B (DCH)	Q (FI)
IPM buffer	0	0	0
	0	1	0
	1	0	0
	1	1	1

Fig. 3 AND logic operation. (A) Symbol of logic gate. (B) Truth table. (C) The normalized fluorescence spectra of logic operation with different inputs. (D) Normalized FI at 471 nm. The concentrations of DCH and BSBOTPE used are 6 μM and 141 μM, respectively. Excitation wavelength was set at 350 nm. n = 3.

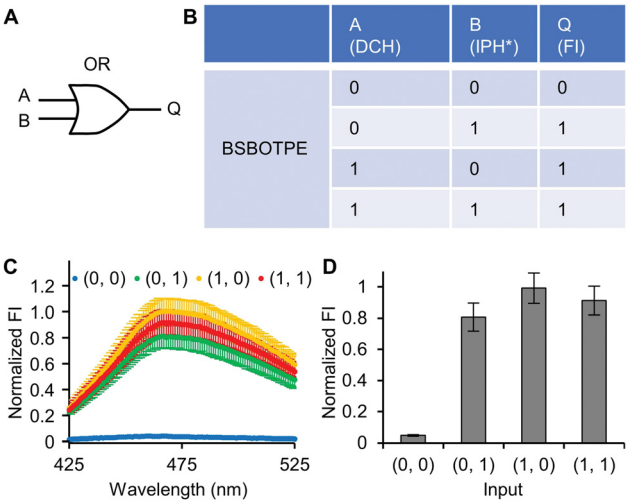

	A (DCH)	B (IPH*)	Q (FI)
BSBOTPE	0	0	0
	0	1	1
	1	0	1
	1	1	1

Fig. 4 OR logic operation. (A) Symbol of logic gate. (B) Truth table. (C) The normalized fluorescence spectra of logic operation with different inputs. (D) Normalized FI at 471 nm. The concentrations of DCH (or IPH*) and BSBOTPE used are 6 μM and 141 μM, respectively. Excitation wavelength was set at 350 nm. n = 3.

capable of self-coacervation and recruitment of charged cargoes,[62–64] as an input. Therefore, we used DCH and IPH*, the macromolecules without and with self-coacervation capability, respectively, as the two inputs to the BSTOPE gate. Incorporation of DCH or IPH* or both exhibited coacervation in complexation with BSBOTPE to generate high FI (output = 1) (Fig. 4C and D). All FI data of Buffer, AND and OR logic operations are consistent with turbidimetry (Fig. S3A–D, ESI†) and confocal laser scanning microscopy (CLSM) (Fig. S4–S7, ESI†).

Next, pre-formed complex coacervates from 'DCH + BSBOTPE' were used as the gate to demonstrate NOT, NAND, NOR and XNOR logic operations. The relative FI at 471 nm is viewed as the output with 0.5 as the threshold value. For a NOT logic operation, the output ('0' or '1') is different from the input ('0' or '1') (Fig. 5A and B). The complex coacervation from DCH and BSBOTPE exhibited high FI signal (output = 1), whilst the employment of mild heating (from 25 °C to 40 °C) dissolved coacervates and reversed the aggregation of BSBOTPE to the dispersed state, thus producing a low FI signal (output = 0) (Fig. 5C and D). Salt can be used as another 'input' to perform NOT logic operation (Fig. S8, ESI†) owing to a charge screening[65] effect. For a NAND logic gate, the output is '0' only if both inputs are '1' (Fig. 6A and B). The *o*-NBA is a photoacid capable of releasing protons upon UV irradiation,[66] thereby engendering the drop of pH[67] (Fig. 6E). Whilst the *o*-NBA or UV light treatment alone had negligible effect on the FI (output = 1), the concurrence thereof triggered a pH drop and protonation of BSBOTPE, thereby disrupting the charge complementary complex coacervation and AIE to produce low FI (output = 0) (Fig. 6C and D). For a NOR logic gate, the output is '1' only if both inputs are '0' (Fig. 7A and B). Heat or salt or both can dissolve the complex coacervation and reverse the aggregation of BSBOTPE to the dispersed state, thereby producing low FI signal (output = 0) (Fig. 7C and D). For a XNOR logic gate, the output is '1' only if the inputs are the same, namely, both are '0' or '1' (Fig. 8A and B). The complex coacervation between DCH and BSBOTPE produces high FI without input (output = 1). With the addition of HCl or NaOH, the protonation of BSBOTPE or the deprotonation of DCH was engendered, respectively, thereby eliminating the charge–complementary complex coacervation and aggregation of BSBOTPE (output = 0). With the addition of both HCl and NaOH, neutralization thereof produced marginal effect (output = 1) (Fig. 8C and D). For NOT, NAND and NOR logic operations, FI data are consistent with turbidimetry (Fig. S3E–H, ESI†) and CLSM (Fig. S9–S12, ESI†). Note that for XNOR logic operation, the FI data are

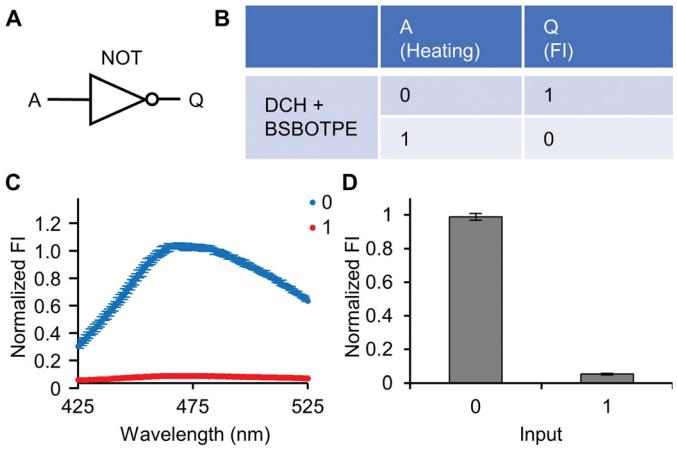

Fig. 5 NOT logic operation. (A) Symbol of logic gate. (B) Truth table. (C) The normalized fluorescence spectra of logic operation with different inputs. (D) Normalized FI at 471 nm. The concentrations of DCH and BSBOTPE used are 6 μM and 141 μM, respectively. Excitation wavelength was set at 350 nm. The 'heat' input is incubated under 40 °C for 2 min. n = 3.

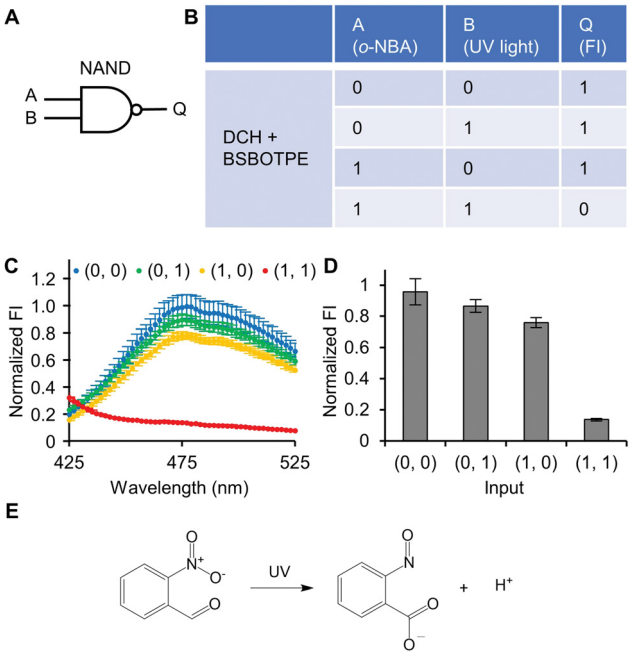

Fig. 6 NAND logic operation. (A) Symbol of logic gate. (B) Truth table. The normalized fluorescence spectra of logic operation with different inputs. (D) Normalized FI at 471 nm. (E) Reaction of *o*-NBA under UV irradiation. DCH stock solution was first heated under 70 °C for 2 min, followed by addition to solvent (150 mM NaCl, 10 wt% PEG 8000, and pH = 7.4) and 15-min maturation under 25 °C. BSBOTPE was then added by inserting minute stock solution, followed by 15-min of incubation. *o*-NBA or/and 365-nm UV light (UVGL-25, Analytik Jena, USA) were applied and incubated for 15 min, followed by 15-min maturation before measurement. The pH of the (1, 1) sample is 6.0, whilst those of the others are 7.4, as is measured by pH-indicator strips. The concentrations of DCH and BSBOTPE used are 6 μM and 141 μM, respectively. Excitation wavelength was set at 350 nm. n = 3.

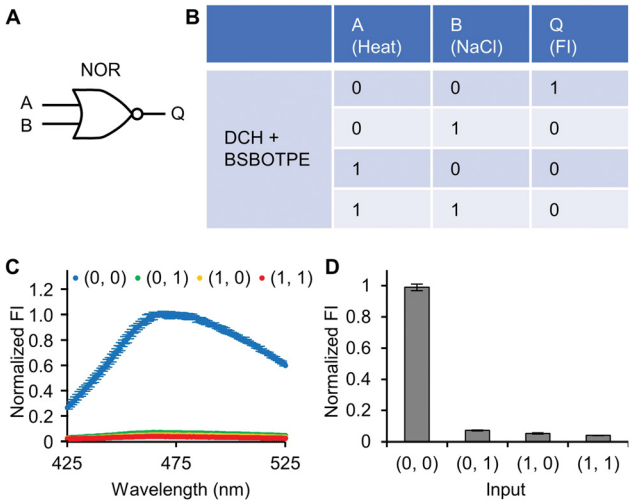

Fig. 7 NOR logic operation. (A) Symbol of logic gate. (B) Truth table. (C) The normalized fluorescence spectra of logic operation with different inputs. (D) Normalized FI at 471 nm. The concentrations of DCH and BSBOTPE used are 6 μM and 141 μM, respectively. Excitation wavelength was set at 350 nm. The 'heat' input is incubation under 40 °C for 2 min. The 'NaCl' input is increasing NaCl concentration from 150 mM to 600 mM, followed by 2-min incubation. n = 3.

consistent with CLSM (Fig. S13, ESI†), whilst there is a mismatch of turbidimetry and FI with the input (0, 1) (Fig. S3I, ESI†), namely, the FI signal is low, whilst the turbidity is high. This surge of turbidity is attributed to the self-coacervation of DCH under alkaline conditions (Fig. S3K, ESI†), which generates little complex coacervation and aggregation of BSBOTPE, resulting in low FI (output = 0).

Further, a mixture of 'DCH + BSBOTPE' was used as the gate to demonstrate XOR logic operations, wherein the relative turbidity is viewed as the output with 0.5 as the threshold value. For a XOR logic gate, the output is '0' only if the inputs are the same, namely, both are '0' or '1' (Fig. 9A and B). Without input, there is only prominent formation of sub-micron-sized droplets, thus resulting in little scattering of visible light and

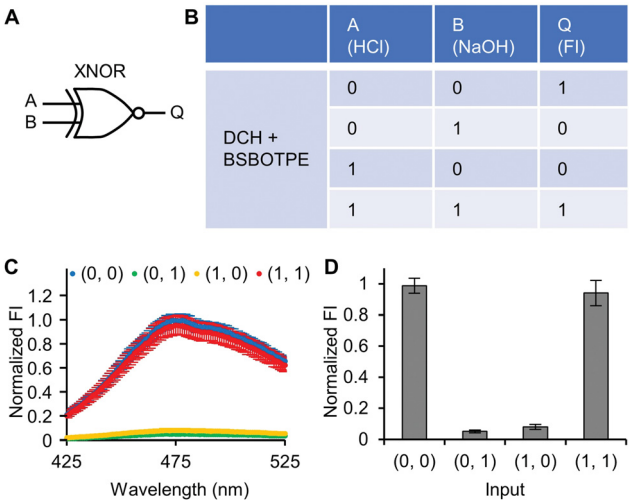

	A (HCl)	B (NaOH)	Q (FI)
DCH + BSBOTPE	0	0	1
	0	1	0
	1	0	0
	1	1	1

Fig. 8 XNOR logic operation. (A) Symbol of logic gate. (B) Truth table. (C) The Normalized fluorescence spectra of logic operation with different inputs. (D) Normalized FI at 471 nm. HCl or NaOH was incorporated by adding stock solution (1 M) at the volume fraction of 2% to adjust the pH from 7.4 to 3.4 or 11.4, respectively, followed by 15-min incubation. The concentrations of DCH and BSBOTPE used are 48 μM and 141 μM, respectively. Excitation wavelength was set at 350 nm. n = 3.

no turbidity (Fig. 9C and Fig. S3J and S14, ESI†) (output = 0). With the input of NaCl to adjust [NaCl] to an intermediate level (1200 mM), there is prominent formation of micron-sized droplets, thus producing extremely high turbidity (Fig. 9C and Fig. S3J and S14, ESI†) (output = 1). With the input of twofold NaCl to adjust [NaCl] to 2400 mM, however, this high ionic strength generates a significant charge screening effect to melt complex coacervation, thereby producing low turbidity (Fig. 9C and Fig. S3J, S14, ESI†) (output = 0). Note that the amount of turbidity does not totally match that of the FI. The low-turbidity-generating input (0, 0) results in high FI, owing to the complex coacervation on the sub-micron scale (Fig. S14 and S15, ESI†). The high-turbidity-generating inputs (0, 1) and (1, 0) result in low FI, owing to the blockage of light transmittance in the bulk solution environment with extremely high turbidity (Fig. S3J, S14 and S15, ESI†), albeit some fluorescence can be seen *via* CLSM (Fig. S14, ESI†).

Lastly, we sought to demonstrate some proof-of-concept applications that employ these molecular logic operations for the further development of organic luminescent materials in aggregation.[68] For information storage and read-out, for example, we applied the 'Buffer (2)' logic operations. A matrix of BSBOTPE (15 μL each, as the gate) was pre-loaded into a 384-well plate, followed by DCH (15 μL each, as the input) loading as a pattern of letters 'HKUST'. This is the information storage process and no pattern can be seen by the naked eye. Upon UV irradiation for information reading, the wells with DCH input emitted intense blue light, resulting into a 'HKUST'-like fluorescent pattern with high signal-to-background ratio (Fig. 10A). To construct a thermo-sensor, for example, we used the solution of complex coacervates from 'DCH + BSBOTPE' as the solvent to prepare dextran hydrogels crosslinked by a vinylsulfone–thiol Michael addition reaction,[57] thereby achieving the 'solidification' of solution-state logic gates (Fig. 10B and ESI†). A solidified 'NOT' logic gate was leveraged for temperature monitoring of the sample solution, whilst the 'output' can

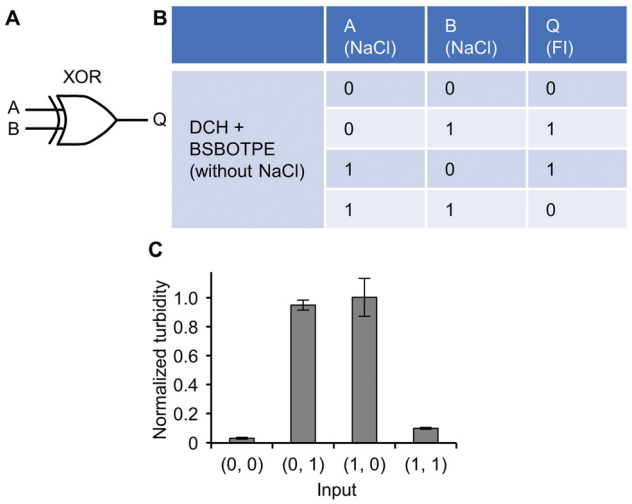

	A (NaCl)	B (NaCl)	Q (FI)
DCH + BSBOTPE (without NaCl)	0	0	0
	0	1	1
	1	0	1
	1	1	0

Fig. 9 XOR logic operation. (A) Symbol of logic gate. (B) Truth table. (C) Normalized turbidity with different inputs. DCH stock solution was first heated under 70 °C for 2 min, followed by addition to solvent (10 mM HEPES, 10 wt% PEG 8000, and pH = 7.4) and 15-min maturation under 25 °C. BSBOTPE was then added by inserting minute stock solution, followed by 15-min incubation. For (0, 1) and (1, 0) inputs, NaCl was incorporated by adding solids (to 1200 mM), followed by 15-min maturation before measurement. The concentrations of DCH and BSBOTPE used are 48 μM and 141 μM, respectively. n = 3.

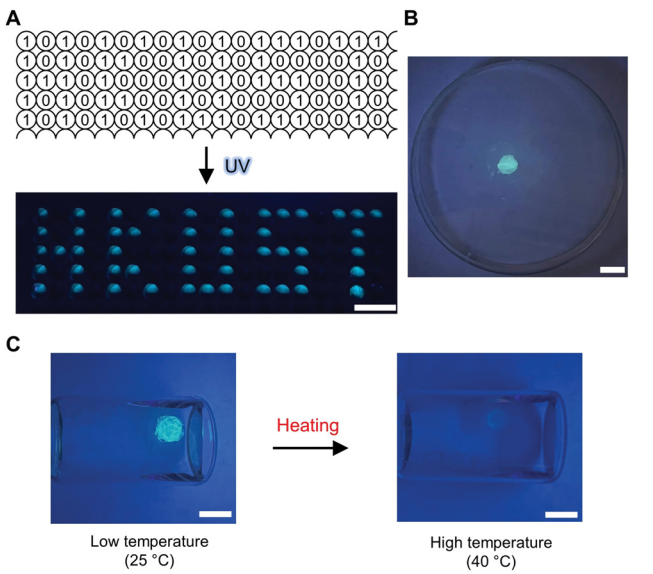

Fig. 10 Application of molecular logic operations. (A) Storage of a 'HKUST' pattern with 'Buffer (2)' gate matrices in a 384-well plate. Top: Schematic illustration of '0' or '1' input to wells. Bottom: Fluorescent pattern 'output'. (B) Solidification of logic gates in a dextran hydrogel. (C) Application of (B) as thermo-sensors in solution. A 365-nm UV lamp was used for excitation. Scale bars, 10 mm.

be easily acquired by the naked eye with the assistance of a portable UV lamp (Fig. 10C).

Conclusions

Leveraging the complex coacervation of polycationic DCH and anionic AIEgen named BSBOTPE, we demonstrated eight basic molecular logic operations with high contrast between Boolean outputs. Environmental stimuli, including heating, pH, ionic strength, ultraviolet light and chemicals (including polycation, IDP-mimetic, bivalent anion and photoacid) were used as either inputs or gates, whilst FI and turbidity were outputs. This work represents a simple yet versatile platform for the execution of molecular logic operations with high contrast between outputs, which can pave the way to the performance of integrated and complicated Boolean operations on the molecular level, which support applications such as information storage and readout media and environmental sensor devices.

Author contributions

Conceptualization: J. L.; investigation: J. L., T. Z. and X. L.; supervision: J. W. Y. L., B. Z. T. and Y. C.; funding acquisition: B. Z. T. and Y. C.; writing – original draft: J. L.; writing – review and editing: J. L., T. Z., X. L., J. W. Y. L., B. Z. T. and Y. C.

Conflicts of interest

There are no conflicts to declare.

Acknowledgements

Financial support was provided by the Hong Kong Research Grant Council (GRF 16102520 and 16103517) and the Innovation and Technology Commission (ITC CNERC14SC01).

Notes and references

1 L. Liu, P. Liu, L. Ga and J. Ai, *ACS Omega*, 2021, **6**, 30189–30204.
2 A. P. de Silva and S. Uchiyama, *Nat. Nanotechnol.*, 2007, **2**, 399–410.
3 J. Andréasson and U. Pischel, *Chem. Soc. Rev.*, 2015, **44**, 1053–1069.
4 A. Muthukrishnan and S. Stroud, *Phys. Rev. A: At., Mol., Opt. Phys.*, 2000, **62**, 052309.
5 X. Cao, X. Zeng, L. Mu, Y. Chen, R. X. Wang, Y. Q. Zhang, J. X. Zhang and G. Wei, *Sens. Actuators, B*, 2013, **177**, 493–499.
6 K. L. Kompa and R. D. Levine, *Proc. Natl. Acad. Sci. U. S. A.*, 2001, **98**, 410–414.
7 A. P. de Silva, S. Uchiyama, T. P. Vance and B. Wannalerse, *Coord. Chem. Rev.*, 2007, **251**, 1623–1632.
8 S. Uchiyama, N. Kawai, A. P. De Silva and K. Iwai, *J. Am. Chem. Soc.*, 2004, **126**, 3032–3033.
9 F. Pu, E. Ju, J. Ren and X. Qu, *Adv. Mater.*, 2014, **26**, 1111–1117.
10 D. Woods, D. Doty, C. Myhrvold, J. Hui, F. Zhou, P. Yin and E. Winfree, *Nature*, 2019, **567**, 366–372.
11 C. Mao, T. H. LaBean, J. H. Reif and N. C. Seeman, *Nature*, 2000, **407**, 493–496.
12 A. P. de Silva, *Molecular Logic-based Computation*, The Royal Society of Chemistry, 2012.
13 N. Cheng, P. Zhu, Y. Xu, K. Huang, Y. Luo, Z. Yang and W. Xu, *Biosens. Bioelectron.*, 2016, **84**, 1–6.
14 A. Bader and S. L. Cockroft, *Chem. – Eur. J.*, 2018, **24**, 4820–4824.
15 X. Lin, Y. Liu, J. Deng, Y. Lyu, P. Qian, Y. Li and S. Wang, *Chem. Sci.*, 2018, **9**, 1774–1781.
16 M. Kluciar, R. Ferreira, B. De Castro and U. Pischel, *J. Org. Chem.*, 2008, **73**, 6079–6085.
17 Y. Shiraishi, Y. Tokitoh and T. Hirai, *Chem. Commun.*, 2005, 5316–5318.
18 A. P. De Silva, M. R. James, B. O. F. McKinney, D. A. Pears and S. M. Weir, *Nat. Mater.*, 2006, **5**, 787–790.
19 J. F. Callan, A. P. De Silva and N. D. McClenaghan, *Chem. Commun.*, 2004, 2048–2049.
20 S. Kou, N. L. Han, D. Van Noort, K. M. K. Swamy, H. K. So, H. S. Jung, K. M. Lee, S. W. Nam, J. Yoon and S. Park, *Angew. Chem., Int. Ed.*, 2008, **47**, 872–876.
21 M. Privman, T. K. Tarn, M. Pita and E. Katz, *J. Am. Chem. Soc.*, 2009, **131**, 1314–1321.
22 J. Chen, J. Pan and C. Liu, *Anal. Chem.*, 2020, **92**, 6173–6180.
23 M. Massey, I. L. Medintz, M. G. Ancona and W. R. Algar, *ACS Sens.*, 2017, **2**, 1205–1214.
24 A. Saghatelian, N. H. Völcker, K. M. Guckian, V. S. Y. Lin and M. R. Ghadiri, *J. Am. Chem. Soc.*, 2003, **125**, 346–347.
25 L. Wang, Y. Zhang and Y. Dong, *Sensors*, 2018, **18**, 3280.
26 Y. Ma, X. Jin, Y. Xing, G. Ni and J. Peng, *Anal. Methods*, 2019, **11**, 2033–2040.
27 H. Liu, Y. Zhou, Y. Yang, W. Wang, L. Qu, C. Chen, D. Liu, D. Zhang and D. Zhu, *J. Phys. Chem. B*, 2008, **112**, 6893–6896.
28 A. Coskun, E. Deniz and E. U. Akkaya, *Org. Lett.*, 2005, **7**, 5187–5189.
29 S. Wang, J. Sun, J. Zhao, S. Lu and X. Yang, *Anal. Chem.*, 2018, **90**, 3437–3442.
30 M. Asakawa, P. R. Ashton, V. Balzani, A. Credi, G. Mattersteig, O. A. Matthews, M. Montalti, N. Spencer, J. F. Stoddart and M. Venturi, *Chem. – Eur. J.*, 1997, **3**, 1992–1996.
31 M. Kumar, R. Kumar and V. Bhalla, *Tetrahedron Lett.*, 2010, **51**, 5559–5562.
32 M. Schmittel, P. Mal and A. De Los Rios, *Chem. Commun.*, 2010, **46**, 2031–2033.
33 M. Zhou, F. Wang and S. Dong, *Electrochim. Acta*, 2011, **56**, 4112–4118.
34 A. Prasanna De Silva and N. D. McClenaghan, *J. Am. Chem. Soc.*, 2000, **122**, 3965–3966.
35 D. Gust, T. A. Moore and A. L. Moore, *Chem. Commun.*, 2006, 1169–1178.
36 P. A. De Silva, N. H. Q. Gunaratne and C. P. McCoy, *Nature*, 1993, **364**, 42–44.
37 J. Luo, Z. Xie, Z. Xie, J. W. Y. Lam, L. Cheng, H. Chen, C. Qiu, H. S. Kwok, X. Zhan, Y. Liu, D. Zhu and B. Z. Tang, *Chem. Commun.*, 2001, 1740–1741.

38 Y. Hong, J. W. Y. Lam and B. Z. Tang, *Chem. Soc. Rev.*, 2011, **40**, 5361–5388.
39 J. Mei, N. L. C. Leung, R. T. K. Kwok, J. W. Y. Lam and B. Z. Tang, *Chem. Rev.*, 2015, **115**, 11718–11940.
40 J. Mei, Y. Hong, J. W. Y. Lam, A. Qin, Y. Tang and B. Z. Tang, *Adv. Mater.*, 2014, **26**, 5429–5479.
41 H. Wang, E. Zhao, J. W. Y. Lam and B. Z. Tang, *Mater. Today*, 2015, **18**, 365–377.
42 S. Deshpande, F. Brandenburg, A. Lau, M. G. F. Last, W. K. Spoelstra, L. Reese, S. Wunnava, M. Dogterom and C. Dekker, *Nat. Commun.*, 2019, **10**, 1–11.
43 C. P. Brangwynne, C. R. Eckmann, D. S. Courson, A. Rybarska, C. Hoege, J. Gharakhani, F. Jülicher and A. A. Hyman, *Science*, 2009, **324**, 1729–1732.
44 S. F. Banani, H. O. Lee, A. A. Hyman and M. K. Rosen, *Nat. Rev. Mol. Cell Biol.*, 2017, **18**, 285–298.
45 J. Liu, F. Zhorabek and Y. Chau, *arXiv Prepr. arXiv2104.10927*.
46 A. A. Hyman, C. A. Weber and F. Jülicher, *Annu. Rev. Cell Dev. Biol.*, 2014, **30**, 39–58.
47 S. Alberti, A. Gladfelter and T. Mittag, *Cell*, 2019, **176**, 419–434.
48 H. Wu and M. Fuxreiter, *Cell*, 2016, **165**, 1055–1066.
49 J. A. Riback, L. Zhu, M. C. Ferrolino, M. Tolbert, D. M. Mitrea, D. W. Sanders, M.-T. Wei, R. W. Kriwacki and C. P. Brangwynne, *Nature*, 2020, **581**, 209–214.
50 J. Liu, R. Feng and Y. Chau, *Matter*, 2022, **5**, 1637–1639.
51 Y. Shin and C. P. Brangwynne, *Science*, 2017, **357**, eaaf4382.
52 C. E. Sing and S. L. Perry, *Soft Matter*, 2020, **16**, 2885–2914.
53 C. S. Cummings and A. C. Obermeyer, *Biochemistry*, 2018, **57**, 314–323.
54 E. Kizilay, A. B. Kayitmazer and P. L. Dubin, *Adv. Colloid Interface Sci.*, 2011, **167**, 24–37.
55 W. M. Babinchak, B. K. Dumm, S. Venus, S. Boyko, A. A. Putnam, E. Jankowsky and W. K. Surewicz, *Nat. Commun.*, 2020, **11**, 1–15.
56 P. Thandapani, T. R. O'Connor, T. L. Bailey and S. Richard, *Mol. Cell*, 2013, **50**, 613–623.
57 J. Liu, R. Ni and Y. Chau, *Chem. Commun.*, 2019, **55**, 7093–7096.
58 Y. Hong, J. W. Y. Lam and B. Z. Tang, *Chem. Commun.*, 2009, 4332–4353.
59 K. Reiche, J. Hartl, A. Blume and P. Garidel, *Biophys. Chem.*, 2017, **220**, 7–19.
60 H. Kim, B. Jin Jeon, S. Kim, Y. S. Jho and D. S. Hwang, *Polymers*, 2019, **11**, 691.
61 T. Maji, S. Banerjee, Y. Biswas and T. K. Mandal, *Macromolecules*, 2015, **48**, 4957–4966.
62 J. Liu, F. Zhorabek, X. Dai, J. Huang and Y. Chau, *ACS Cent. Sci.*, 2022, **8**, 493–500.
63 J. Liu, F. Zhorabek and Y. Chau, *ACS Macro Lett.*, 2022, **32**, 562–567.
64 J. Liu, F. Zhorabek, T. Zhang, J. W. Y. Lam, B. Z. Tang and Y. Chau, *Small*, 2022, **18**, 2201721.
65 C. D. Keating, *Acc. Chem. Res.*, 2012, **45**, 2114–2124.
66 J. M. Allen, S. K. Allen and S. W. Baertschi, *J. Pharm. Biomed. Anal.*, 2000, **24**, 167–178.
67 Y. Gao and M. J. Serpe, *ACS Appl. Mater. Interfaces*, 2014, **6**, 8461–8466.
68 J. Yang, M. Fang and Z. Li, *Aggregate*, 2020, **1**, 6–18.